Performance Comparison of Typical Frequency Response Strategies for Power Systems with High Penetration of Renewable Energy Sources

Liansong Xiong, *Senior Member, IEEE,* Xiaokang Liu, *Member, IEEE,* Hongqing Liu, and Yonghui Liu, *Student Member, IEEE*

***Abstract*—Droop control, inertia control, and PD control are three typical frequency response (FR) strategies of grid-tied inverters interfaced renewable energy sources (RES) to restrain the power system frequency indicators, i.e., frequency deviation ($\Delta\omega$) and the rate of change of frequency (RoCoF). Due to the highly limited inverter capacity, the FR performance in power systems with high RES penetration should be optimized. To this end, this paper first analyzes the impact of high-penetration renewable energy injection on power system frequency stability, and derives the system frequency expressions in the absence of an FR scheme, and in the presence of droop/inertia/PD controls that are representative for various virtual synchronous generator-based FR schemes. Under the same constraint of available FR capacity, control parameter ranges of these FR schemes are obtained, and their optimal conditions for restraining the maxima of $\Delta\omega$ and RoCoF are identified and compared analytically. Comparison conclusions are finally proved by the provided experiment and simulation results.**

***Index Terms*—Frequency response (FR), frequency deviation, rate of change of frequency (RoCoF), renewable energy sources (RES), grid-tied inverter, limited inverter capacity.**

I. Introduction

TO tackle the environmental problems caused by the use of traditional fossil energy, there has been a drastically emerging trend across the globe to adopt renewable, clean energy generation technologies, encompassing wind, solar, and heat, etc. As the proportion of renewable energy sources (RES) within the power system continues to increase, the system operation has observed notable changes [1]. The volatility and intermittency of RES have caused the power system uncertainty on both source- and load-sides; at the same time, the large-scale replacement of synchronous generator (SG) interfaced traditional power plants by grid-tied inverter interfaced RES has led to reduced system equivalent inertia and weakened damping ability [2], impairing the system frequency response (FR) ability and inducing huge challenges to the power system frequency stability [3].

When a power system with high penetration of RES is subjected to random disturbances, its frequency deviation ($\Delta\omega$) and rate of change of frequency (RoCoF) are prone to large fluctuations, which can cause a variety of consequences to the power system. To avoid this, the grid code in many countries limits the grid $\Delta\omega$ and RoCoF by adopting relays: once an indicator, $\Delta\omega$ or RoCoF, exceeds its threshold for a certain time, its related load shedding or generator disconnection relays will be triggered. As illustrative examples, China, Ireland, Australia, and the UK accept the frequency nadir above 49.0 Hz, 47.5 Hz, 47.5 Hz, and 49.5 Hz, respectively. Typical RoCoF relays in 50 Hz systems are set between 0.1 and 1.0 Hz/s [4].

An SG with large inertia has notable FR ability, viz., it can autonomously adjust the output power based on system frequency dynamics and hinder the frequency change [4]. Therefore, the high-inertia power system with SGs as its major constitution has a more robust frequency, and its $\Delta\omega$ and RoCoF easily satisfy the grid code requirements. Conversely, when disturbed, the low-inertia power system with a high proportion of RES is prone to significant $\Delta\omega$ and RoCoF, which must be reduced to avoid triggering frequency-related relays. In the latter case, the grid-tied inverters are required to provide additional FR function analogous to the SGs [5], by use of various FR strategies.

Existing FR strategies mainly encompass the virtual inertia control [6], the PD control [7], the virtual synchronous machine [8], the synchronverter [9], the synchronous power control [10], the generalized droop control [11], etc. In [12], an improved inverter droop control strategy is proposed to achieve frequency stability of the microgrid. In [13], the VSG control is coordinated with the motor speed control, such that the grid frequency demand is quickly responded to by the kinetic energy stored in the rotating motor load, in the absence of the energy storage equipment. However, designing parameters used by these methods requires insights into the grid inertia/damping parameters and random disturbances that are difficult to predict in advance. To solve this issue, [3] proposed a more practical frequency trajectory based strategy to improve the frequency stability of standalone power systems; by using this strategy, the inverter can provide only the lacking inertia and damping to the system. These frameworks generally enable inverters to provide the FR power proportional to $\Delta\omega$ and/or RoCoF, which can be viewed equivalent to the classic and widely used droop, inertia, or PD control. As an example, the equivalence of the frequency droop control and VSG control under certain conditions is demonstrated in [14]. Accordingly, increasing the controller gain ideally indicates more FR power and a further reduction in $\Delta\omega$ and RoCoF. However, for a grid-tied inverter, the majority of its designed capacity has been allocated to and used for its core function, i.e., transmitting desired power to the grid. As a result, the available capacity for FR service is extremely limited, and increasing controller gains easily leads to an overcurrent fault.

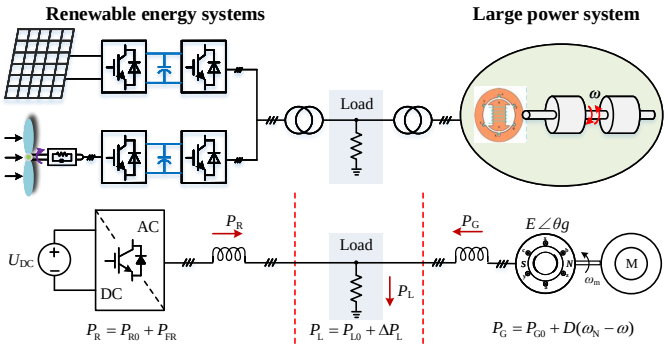

Fig. 1. Schematic diagram of a power system with renewable energy injection.

Overall, it is of paramount importance to identify the most efficient FR strategy in terms of $\Delta\omega$ and RoCoF suppression, under the same constraint of insufficient available capacity of the inverter. This is done in this work by comparing the typical FR schemes, and the conclusions can throw light on efficient FR scheme selection in a particular scenario.

II. FR Features of Power Systems with RESs

With the aim of interpreting the influence of RES proportion on system frequency features, this manuscript first establishes the FR models of power systems with RES integration.

A. Power Systems with RES Integration

As shown in Fig. 1, RES, including wind turbines, photovoltaics, wave energy, etc., are generally connected to power systems comprising conventional energy sources (e.g., thermal, hydraulic, and nuclear powers) through grid-tied inverters. Accordingly, these power systems encompass inverters and synchronous machines as their main equipment.

To analyze the impact of RES based generations on the operating features of power system, the penetration level of the RES, σ, is defined as the ratio of the total RES generation power P_{R} to the total load power P_{L}, i.e., $\sigma = P_{\mathrm{R}}/P_{\mathrm{L}}$.

In the steady state, the power system maintains a power balance between supply and demand, yielding

$$P_{\mathrm{G0}} + P_{\mathrm{R0}} = P_{\mathrm{L0}} \tag{1}$$

where P_{G0}, P_{R0}, and P_{L0} are the traditional energy power, the RES power and the load power in the steady state, respectively.

When a grid disturbance (e.g., a sudden load power increase of ΔP_{L}) occurs, the power balance condition given by (1) is no longer valid. The grid frequency will change accordingly, and components in the grid will react to the frequency change at the same time. The grid frequency variation features driven by unbalanced active power are usually denoted as FR characteristics of the power system.

The FR process of power grid generally involves three stages, [15], [16], as shown in Fig. 2. Specifically,

1) Stage I: *inertia response* is the natural responding mechanism of SGs that requires no human interaction, and provides the short-term impulsive power support with a typical action time within 5 seconds after the disturbance. It automatically functions on the system frequency change, and the pertinent output power is proportional to the RoCoF index. The larger the equivalent inertia of the system, the slower the system frequency change, and the smaller the RoCoF index.

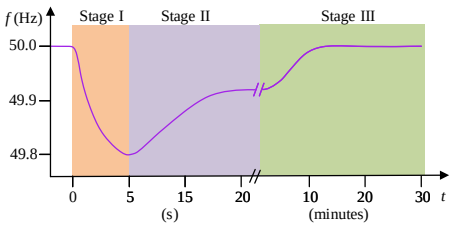

Fig. 2. FR process of a power system.

Since Stage I is critical for frequency indicators, the grid FR control is possibly needed during this stage to limit the $\Delta\omega$ and RoCoF and prevent the frequency-based relays from being triggered.

2) The grid will enter Stage II: *primary frequency regulation* when the frequency deviation exceeds a specified threshold, and after the power plants start the frequency regulation function (usually 5–15 s depending on the mechanical process). The generators automatically adjust their valves to reduce the grid imbalance power, thereby suppressing the frequency deviation. This stage has a common duration of 5–30 s. However, Stage II is an error-tolerate control, namely, the resulting steady-state frequency still exhibits a certain deviation that occasionally fails to satisfy the frequency quality requirements.

3) Stage III: *secondary frequency regulation* will be started by partial power plants, with the aim of balancing the generation and load power of the system and resuming the nominal frequency. As a rule of thumb, this process starts several minutes after the disturbance.

B. FR Process Modeling of Power System

To analyze grid FR characteristics, frequency ω, and its influential factors in the initial stage, the dynamic response of ω is modeled first.

For ease of analysis, a power system is usually represented by an equivalent power generation unit connected to an equivalent load, whose power equals the total load power, P_{L}. The inertia of the equivalent power grid is synthesized as [17]

$$H = \frac{\sum H_i P_i}{\sum P_{\mathrm{L}i}} = \frac{\sum H_i P_{\mathrm{i}}}{P_{\mathrm{L}}} \tag{2}$$

where P_i and H_i are the generated power and inertia coefficient of the i-th power generation unit, respectively, and $P_{\mathrm{L}i}$ is the power consumption of the i-th load.

1) Case A ($\sigma = 0$ or $\sigma = 1$): When $\sigma = 0$, namely, $P_{\mathrm{R}} = 0$, the power system contains null RES, and the load power is fully provided by traditional SGs, yielding

$$P_{\mathrm{L}} = \sum P_{\mathrm{L}i} = \sum P_i = \sum P_{\mathrm{G}i} = P_{\mathrm{G}} \tag{3}$$

where $P_{\mathrm{G}i}$ and P_{G} are the generated powers of the i-th SG and the aggregated equivalent generator, respectively.

According to (2) and (3), the equivalent inertia of the power grid in the absence of RES integration is

$$H_0 = \frac{\sum H_{\mathrm{G}i} P_{\mathrm{G}i}}{P_{\mathrm{L}}} \tag{4}$$

where $H_{\mathrm{G}i}$ is the inertia coefficient of the i-th SG.

Analogously, if the power system is formed of RES, i.e., $\sigma = 1$ and $P_{\mathrm{G}} = 0$, its equivalent inertia writes

$$H_{\mathrm{R}} = \frac{\sum H_{\mathrm{R}i} P_{\mathrm{R}i}}{P_{\mathrm{L}}} \tag{5}$$

where $P_{\mathrm{R}i}$ and $H_{\mathrm{R}i}$ are the generated power and inertia coefficient of the i-th RES generator, respectively.

Compared to the SG inertia provided by the main shaft of steam/hydraulic turbine, the RES inertia that mainly roots from the rotor of wind turbine and the DC-link capacitance of inverter is negligible [18]. Namely, $H_{\mathrm{R}i} \approx 0$.

2) Case B ($0 < \sigma < 1$): In this case, $P_{\mathrm{R}} \neq 0$, and the power system involves a certain proportion of RES, as shown in Fig. 1. It is

$$\sum P_{\mathrm{R}i} = P_{\mathrm{R}} = \sigma P_{\mathrm{L}} \tag{6}$$

$$\sum P_{\mathrm{G}i} = P_{\mathrm{G}} = (1-\sigma) P_{\mathrm{L}} \tag{7}$$

By substituting (6) and (7) into (4) and (5), the equivalent inertia of the power grid can be expressed as

$$\begin{aligned} H &= \frac{\sum H_i P_i}{\sum P_{\mathrm{L}i}} = \frac{\sum H_{\mathrm{R}i} P_{\mathrm{R}i} + \sum H_{\mathrm{G}i} P_{\mathrm{G}i}}{P_{\mathrm{L}}} \\ &= (1-\sigma) H_0 + \sigma H_R \approx (1-\sigma) H_0 \end{aligned} \tag{8}$$

Similarly, damping coefficients of SGs and frequency interactive loads can be joined into an equivalent coefficient D, i.e., the system damping power can be modeled as $D(\omega_{\mathrm{N}} - \omega)$.

Hence, by assuming the damping coefficient of the power system without RES to be D_0, the equivalent damping parameter of the RES-integrated grid can be approximated as

$$D \approx D_0 (1-\sigma) \tag{9}$$

Let us consider a disturbance of sudden load change by ΔP_{L}. As previously discussed, the speed governors and prime movers of traditional generations with sufficient FR capacity cannot be timely enabled during Stage I (in seconds), and are hence neglected in this initial stage. Accordingly, the dynamic frequency equation of the system can be written as

$$2H \frac{\mathrm{d}\omega}{dt} = P_{\mathrm{R0}} + P_{\mathrm{FR}} + P_{\mathrm{G0}} + D(\omega_{\mathrm{N}} - \omega) - (P_{\mathrm{L0}} + \Delta P_{\mathrm{L}}) \tag{10}$$

where P_{FR} is the FR power output by RES according to the grid frequency deviation ($\Delta\omega$) and RoCoF indicators.

By considering (1), (10) can be simplified to

$$2H \frac{\mathrm{d}\omega}{dt} = P_{\mathrm{FR}} + D(\omega_{\mathrm{N}} - \omega) - \Delta P_{\mathrm{L}} \tag{11}$$

C. Effect of RES Penetration Level on Grid FR Features

RES usually operate in the constant power mode and do not respond to grid frequency changes, i.e., $P_{\mathrm{FR}} = 0$. In this case, by substituting (8) and (9) into (11), the dynamic equation of power system frequency with RES penetration level of σ can be obtained, yielding

$$2(1-\sigma) H_0 \frac{\mathrm{d}\omega_{\mathrm{NO}}}{dt} = (1-\sigma) D_0 (\omega_{\mathrm{N}} - \omega_{\mathrm{NO}}) - \Delta P_{\mathrm{L}} \tag{12}$$

Solution to (12) yields

$$\omega_{\mathrm{NO}} = \omega_{\mathrm{N}} - \frac{\Delta P_{\mathrm{L}}}{(1-\sigma) D_0} \left(1 - e^{-\frac{D_0}{2H_0} t}\right) \tag{13}$$

From (13), $\Delta\omega$ and RoCoF of the grid, in the absence of the FR service provided by RES, can be derived as

$$\Delta\omega_{\mathrm{NO}} = \omega_{\mathrm{N}} - \omega_{\mathrm{NO}} = \frac{\Delta P_{\mathrm{L}}}{(1-\sigma) D_0} \left(1 - e^{-\frac{D_0}{2H_0} t}\right) \tag{14}$$

$$R_{\mathrm{NO}} = \left| \frac{\mathrm{d}\omega_{\mathrm{NO}}}{\mathrm{d}t} \right| = \frac{\Delta P_{\mathrm{L}}}{2(1-\sigma) H_0} e^{-\frac{D_0}{2H_0} t} \tag{15}$$

It is apparent that the disturbance ΔP_{L} leads to inevitable changes in the system frequency ω, and further induces issues of frequency deviation and RoCoF. According to (14) and (15), the maxima of $\Delta\omega$ and RoCoF can be derived as

$$\Delta\omega_{\mathrm{NO}}|_{\max} = \lim_{t\to\infty} \Delta\omega_{\mathrm{NO}} = \frac{\Delta P_{\mathrm{L}}}{(1-\sigma) D_0} \tag{16}$$

$$R_{\mathrm{NO}}|_{\max} = \lim_{t\to 0} R_{\mathrm{NO}} = \frac{\Delta P_{\mathrm{L}}}{2(1-\sigma) H_0} \tag{17}$$

(8), (9), (16), and (17) show that: with the increase of the RES penetration level, the equivalent inertia and damping effects of the power grid decrease linearly. With the same disturbance power, ΔP_{L}, a higher penetration rate of RES (σ) causes larger $\Delta\omega$ and RoCoF values and elevated adverse impact on the grid FR characteristics, which jeopardize the safety and stability of the grid frequency. If $\Delta\omega$ or RoCoF exceeds the threshold, load shedding or generator disconnection relays will be triggered [19]. Hence, grid-tied inverters of RES cannot maintain the constant power mode, yet must respond to grid frequency changes and provide FR services as necessary.

III. Typical FR Schemes and Comparison

With existing FR schemes, the energy from DC capacitors of inverters [20], rotors of wind turbines [21], RES with operating reserves [22], and RES with energy storage devices [23] including batteries, supercapacitors, etc, are fully exploited to provide the necessary FR service when the power grid suffers from large disturbances. The FR energy needs to be sent to the grid through the interfacing inverters of RES and the FR power P_{FR} is generally proportional to $\Delta\omega$ and/or RoCoF.

Therefore, the existing FR schemes can be simplified to the classic droop, inertia, and PD controls. When these control schemes are adopted (see Fig. 3 for a typical control diagram), the pertinent FR powers are denoted as P_{D}, P_{I}, and P_{pd}, respectively, and can be calculated as

$$\begin{cases} P_{\mathrm{D}} = K_{\mathrm{D}} (\omega_{\mathrm{N}} - \omega_{\mathrm{D}}) \\ P_{\mathrm{I}} = s K_{\mathrm{I}} (\omega_{\mathrm{N}} - \omega_{\mathrm{I}}) \\ P_{\mathrm{pd}} = (K_{\mathrm{p}} + s K_{\mathrm{d}}) (\omega_{\mathrm{N}} - \omega_{\mathrm{pd}}) \end{cases} \tag{18}$$

where, K_{D} and K_{I} are controller gains of droop control and inertia control, respectively. K_{p} and K_{d} are controller gains of PD control, respectively.

Here, particular emphasis is placed on the limitation of inverter power, viz., the provided FR power must not exceed the inverter idle capacity P_{m} ($0 \le P_{\mathrm{FR}} \le P_{\mathrm{m}}$). It is also assumed $P_{\mathrm{m}} < \Delta P_{\mathrm{L}}$ hereinafter and the power disturbance

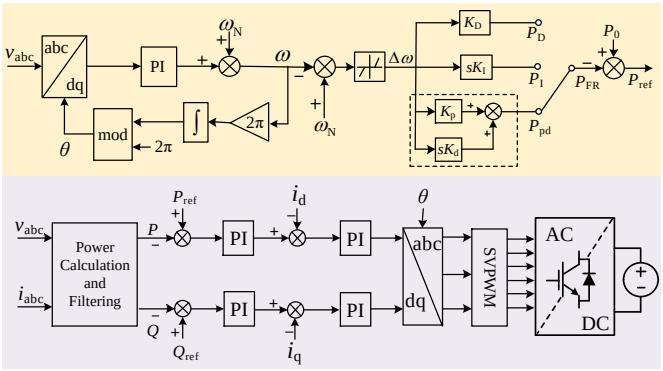

Fig. 3. Control diagram of FR with various FR schemes.

will be thoroughly compensated by the SG based power plants in the following Stage II and Stage III (see Fig. 2).

By substituting (18) into (11) to replace P_{FR}, the system frequency under the three FR strategies can be obtained as

$$\begin{cases} \omega_{\text{D}} = \omega_{\text{N}} - \dfrac{\Delta P_{\text{L}}}{D+K_{\text{D}}}\left(1-e^{-\frac{D+K_{\text{D}}}{2H}t}\right) \\ \omega_{\text{I}} = \omega_{\text{N}} - \dfrac{\Delta P_{\text{L}}}{D}\left(1-e^{-\frac{D}{2H+K_{\text{I}}}t}\right) \\ \omega_{\text{pd}} = \omega_{\text{N}} - \dfrac{\Delta P_{\text{L}}}{K_{\text{p}}+D}\left(1-e^{-\frac{K_{\text{p}}+D}{2H+K_{\text{d}}}t}\right) \end{cases} \tag{19}$$

The pertinent grid $\Delta\omega$ and RoCoF maxima are

$$\begin{cases} \Delta\omega_{\text{D}}|_{\max} = \lim\limits_{t\to\infty}\Delta\omega_{\text{D}} = \dfrac{\Delta P_{\text{L}}}{D+K_{\text{D}}} < \Delta\omega_{\text{NO}}|_{\max} \\ \Delta\omega_{\text{I}}|_{\max} = \lim\limits_{t\to\infty}\Delta\omega_{\text{I}} = \dfrac{\Delta P_{\text{L}}}{D} = \Delta\omega_{\text{NO}}|_{\max} \\ \Delta\omega_{\text{pd}}|_{\max} = \lim\limits_{t\to\infty}\Delta\omega_{\text{pd}} = \dfrac{\Delta P_{\text{L}}}{K_{\text{p}}+D} < \Delta\omega_{\text{NO}}|_{\max} \end{cases} \tag{20}$$

$$\begin{cases} R_{\text{D}}|_{\max} = \lim\limits_{t\to 0}\left|\dfrac{\text{d}\omega_{\text{D}}}{\text{d}t}\right| = \dfrac{\Delta P_{\text{L}}}{2H} = R_{\text{NO}}|_{\max} \\ R_{\text{I}}|_{\max} = \lim\limits_{t\to 0}\left|\dfrac{\text{d}\omega_{\text{I}}}{\text{d}t}\right| = \dfrac{\Delta P_{\text{L}}}{2H+K_{\text{I}}} < R_{\text{NO}}|_{\max} \\ R_{\text{pd}}|_{\max} = \lim\limits_{t\to 0}\left|\dfrac{\text{d}\omega_{\text{pd}}}{\text{d}t}\right| = \dfrac{\Delta P_{\text{L}}}{2H+K_{\text{d}}} < R_{\text{NO}}|_{\max} \end{cases} \tag{21}$$

Comparing i) (16) and (20), and ii) (17) and (21), it is seen that: in the presence of the same disturbance ΔP_{L}, a) the droop control equivalently increases the system damping coefficient from D to $D+K_{\text{D}}$, hence reduces $\Delta\omega$; b) the inertia control effectively increases the system inertia coefficient from $2H$ to $2H+K_{\text{I}}$, hence reduces RoCoF; c) the PD control increases the system damping ability and inertia effect simultaneously, and reduces both $\Delta\omega$ and RoCoF. Besides, large controller gains contribute to a further reduction in $\Delta\omega$ and RoCoF.

By substituting (19) into (18), P_{FR} with the three FR strategies are obtained. For the PD control, it is

$$P_{\text{pd}} = \frac{K_{\text{p}}\Delta P_{\text{L}}}{K_{\text{p}}+D} + \frac{\left(K_{\text{d}}D-2HK_{\text{p}}\right)\Delta P_{\text{L}}}{\left(2H+K_{\text{d}}\right)\left(K_{\text{p}}+D\right)}e^{-\frac{K_{\text{p}}+D}{2H+K_{\text{d}}}t} \tag{22}$$

Accordingly, its maximum level is

$$P_{\text{pd}}|_{\max} = \begin{cases} \lim\limits_{t\to 0}P_{\text{pd}} = \dfrac{K_{\text{d}}\Delta P_{\text{L}}}{2H+K_{\text{d}}} \le P_{\text{m}} & \dfrac{D}{2H} > \dfrac{K_{\text{p}}}{K_{\text{d}}} \\ \lim\limits_{t\to\infty}P_{\text{pd}} = \dfrac{K_{\text{p}}\Delta P_{\text{L}}}{K_{\text{p}}+D} \le P_{\text{m}} & \dfrac{D}{2H} \le \dfrac{K_{\text{p}}}{K_{\text{d}}} \end{cases} \tag{23}$$

The pertinent controller gains satisfy

$$\frac{2HK_{\text{p}}}{D} < K_{\text{d}} \le \frac{2HP_{\text{m}}}{\Delta P_{\text{L}}-P_{\text{m}}} \tag{24}$$

or

$$\frac{DK_{\text{d}}}{2H} \le K_{\text{p}} \le \frac{DP_{\text{m}}}{\Delta P_{\text{L}}-P_{\text{m}}} \tag{25}$$

From (18), to maximize the provided FR power, the PD controller gains should take the maxima of (24) and (25), viz.

$$\begin{cases} K_{\text{p}} = \dfrac{DP_{\text{m}}}{\Delta P_{\text{L}}-P_{\text{m}}} \\ K_{\text{d}} = \dfrac{2HP_{\text{m}}}{\Delta P_{\text{L}}-P_{\text{m}}} \end{cases} \tag{26}$$

Likewise, FR powers and their maxima provided by the other FR strategies yield

$$\begin{cases} P_{\text{D}}|_{\max} = K_{\text{D}}\lim\limits_{t\to\infty}\Delta\omega_{\text{D}} \le P_{\text{m}} \\ P_{\text{I}}|_{\max} = K_{\text{I}}\lim\limits_{t\to 0}s\Delta\omega_{\text{I}} \le P_{\text{m}} \end{cases} \tag{27}$$

Their controller parameters should take

$$K_{\text{D}} = \frac{DP_{\text{m}}}{\Delta P_{\text{L}}-P_{\text{m}}} \tag{28}$$

$$K_{\text{I}} = \frac{2HP_{\text{m}}}{\Delta P_{\text{L}}-P_{\text{m}}} \tag{29}$$

Substituting (26), (28), and (29) into (19), the grid $\Delta\omega$ and RoCoF maxima are obtained for different FR schemes of the inverter, as

$$\begin{cases} \Delta\omega_{\text{D}}|_{\max} = \lim\limits_{t\to\infty}\Delta\omega_{\text{D}} = \dfrac{\Delta P_{\text{L}}-P_{\text{m}}}{D} < \Delta\omega_{\text{NO}}|_{\max} \\ \Delta\omega_{\text{I}}|_{\max} = \lim\limits_{t\to\infty}\Delta\omega_{\text{I}} = \dfrac{\Delta P_{\text{L}}}{D} = \Delta\omega_{\text{NO}}|_{\max} \\ \Delta\omega_{\text{pd}}|_{\max} = \lim\limits_{t\to\infty}\Delta\omega_{\text{pd}} = \dfrac{\Delta P_{\text{L}}-P_{\text{m}}}{D} < \Delta\omega_{\text{NO}}|_{\max} \end{cases} \tag{30}$$

$$\begin{cases} R_{\text{D}}|_{\max} = \lim\limits_{t\to 0}\left|\dfrac{\text{d}\omega_{\text{D}}}{\text{d}t}\right| = \dfrac{\Delta P_{\text{L}}}{2H} = R_{\text{NO}}|_{\max} \\ R_{\text{I}}|_{\max} = \lim\limits_{t\to 0}\left|\dfrac{\text{d}\omega_{\text{I}}}{\text{d}t}\right| = \dfrac{\Delta P_{\text{L}}-P_{\text{m}}}{2H} < R_{\text{NO}}|_{\max} \\ R_{\text{pd}}|_{\max} = \lim\limits_{t\to 0}\left|\dfrac{\text{d}\omega_{\text{pd}}}{\text{d}t}\right| = \dfrac{\Delta P_{\text{L}}-P_{\text{m}}}{2H} < R_{\text{NO}}|_{\max} \end{cases} \tag{31}$$

Since the grid imbalance power is the underlying reason behind $\Delta\omega$ and RoCoF issues, a reduction of imbalance power improves $\Delta\omega$ and RoCoF indexes. Comparing i) (30) and (20), and ii) (31) and (21), it is seen that the droop and the inertia controls reduce $\Delta\omega$ and RoCoF to the minimum, respectively, since the disturbance power ΔP_{L} is compensated for to the lowest value $\Delta P_{\text{L}}-P_{\text{m}}$, owing to the provided FR power.

In addition, the dynamics of FR power with different schemes, which can be obtained by substituting (19), (26), and (29) into (18), suggest that: for the droop and the inertia

TABLE I
PARAMETERS OF TWO-CONVERTER SYSTEM.

Parameter	Value	Parameter	Value
Rated line-to-line voltage E_0	380 Vrms	Disturbance power	8 kW
Rated grid frequency	50 Hz	Passive filter	0.01 Ω/0.1 mH
Rated grid active power P_{ref}	20 kW	DC voltage U_{DC}	800 V
Rated grid reactive power Q_{ref}	0 kVar	Current loop K_{p}	0.01
Load power	35 kW	Current loop K_{i}	2.5
Active power loop K_{P}	7.6E-5	Voltage loop K_{p}	0.2
Reactive power loop K_{Q}	3.1E-3	Voltage loop K_{i}	36

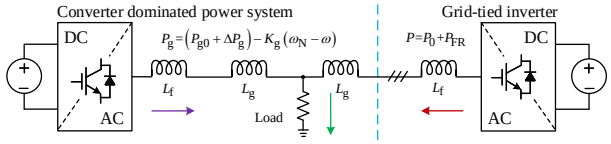

Fig. 4. Configuration of the two-converter experimental system.

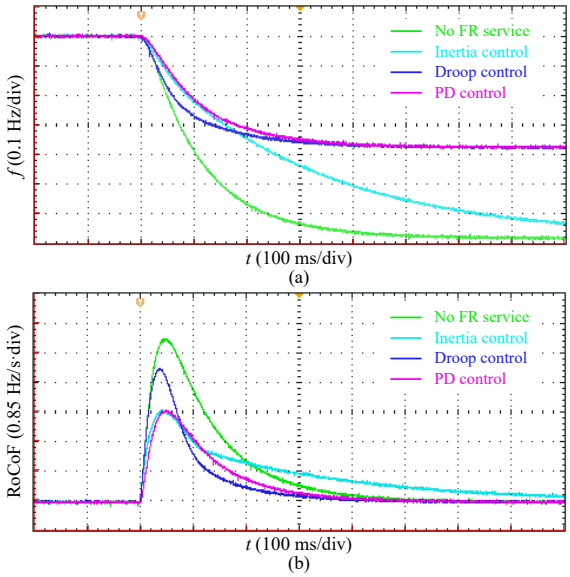

Fig. 5. Results of the two-converter system: (a) frequency and (b) RoCoF.

controls, P_{FR} reaches P_{m} solely in the event of maximum grid $\Delta\omega$ and RoCoF, respectively, whereas the PD control enables the maximum P_{FR} output in the whole interval, maintaining the minimum possible grid imbalance power and drastically reducing both $\Delta\omega$ and RoCoF.

Note that the optimal FR behaviors [i.e., those given by (30) and (31)] are achieved when controller parameters satisfy (26) and (29). Due to the difficulty in determining the power disturbance ΔP_{L} as well as H and D parameters, the optimal FR performance is hardly realized in the practical design. For the PD control, the optimal FR service is provided when P_{pd} is equal to the inverter idle capacity P_{m}. Accordingly, this optimal FR performance can be equivalently achieved regardless of the possibly unknown parameters (e.g., ΔP_{L}, H, and D), by fully utilizing the idle capacity of the inverter, and directly setting the inverter reference FR power to $P_{\text{FR}} = P_{\text{m}}$ when both $\Delta\omega$ and RoCoF are large.

IV. VERIFICATION IN TWO-CONVERTER SYSTEM

In this paper, hardware-in-the-loop (HIL) experiments (see Fig. 4 for system configuration and Table I for main parameters) are first performed in a two-converter system to verify the effectiveness of comparison results. A converter-dominated system with low inertia and weak damping ability is emulated by a droop control based converter (left part of Fig. 4). A RES inverter with the active FR ability yet limited FR capacity (right part of Fig. 4) is connected to the system. Specifically, its steady-state power is 0.8 p.u., and its maximum idle capacity for FR service is 0.2 p.u. A sudden load power increase causes the grid frequency to drop within 0.5 s, in which interval the speed governors and prime movers cannot be enabled (and their models are safely discarded for the HIL emulation). The experiment results with the three FR schemes are shown in Fig. 5. Among them, the optimal FR performances of the droop and the inertia controls are achieved by repeated calibration of controller parameters, whereas a constant output power of 1.0 p.u. is set for the optimal PD control.

From Fig. 5, the frequency drops rapidly in the absence of inverter FR service, resulting in a maximum $\Delta\omega$ of 0.68 Hz and a maximum RoCoF of 4.57 Hz/s. Such a critical case can easily trigger frequency related relays. System frequency is improved when the inverter FR service is provided. Specifically, the maximum $\Delta\omega$ is significantly reduced to 0.38 Hz when the droop or the PD control is used, whereas the inertia control fails to reduce the maximum $\Delta\omega$. The maximum RoCoF values are notably reduced to 2.56 and 2.55 Hz/s, respectively, when the inertia and the PD controls are used; however, the droop control has a limited suppression effect on the maximum RoCoF, which slightly decreased to 3.76 Hz/s.

Besides, the maximum RoCoF is smaller when the droop control is adopted compared to the natural response without the FR service. This can be ascribed to the real-time RoCoF calculation process, viz., a short time duration used for discrete differentiation lowers the calculated maximum RoCoF, whose theoretical value (assuming $t \to 0$) should be larger.

V. VERIFICATION IN IEEE 4M2A SYSTEM

To better validate the comparative results in a realistic and complex system, an IEEE 4-machine-2-area (4M2A) network [24] (see Fig. 6) is investigated through offline simulations, due to the limited performance of the HIL platform. Based on the 4M2A model, the studied network replaces the traditional plant G4 with a 100 MW inverter to emulate the RES integration. A sudden load increase causes the frequency to decrease, and the FR performances of the typical schemes are compared in Fig. 7.

For natural system response without FR service from the grid-tied inverter, the frequency drastically drops during Stage I, due to the low inertia and damping of the system caused by the high penetration of RES. In this case, the frequency nadir reaches 49.37 Hz [see Fig. 7(a)], and the maximum RoCoF reaches 0.5 Hz/s [see Fig. 7(b)]. Frequency protection relays can be easily triggered. After Stage I, the frequency deviation exceeds the threshold for primary frequency regulation. After Stage II, the system frequency eventually stabilizes at 49.79

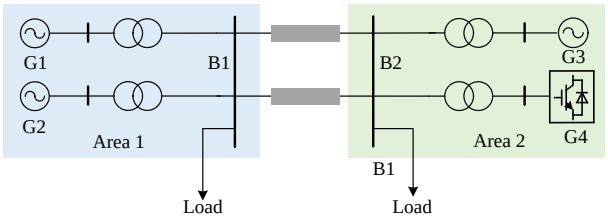

Fig. 6. Configuration of the 4M2A system.

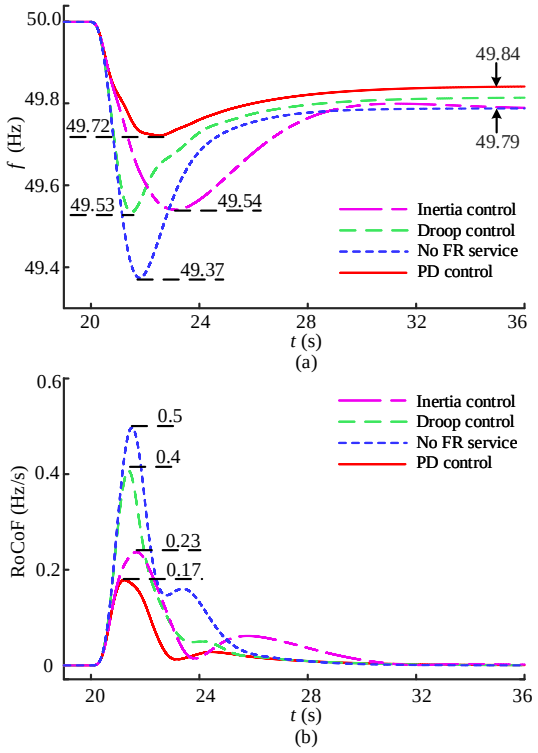

Fig. 7. Results of the 4M2A system: (a) frequency and (b) RoCoF.

Hz, which is still beyond the acceptable range of the steady-state frequency quality, i.e., ± 0.2 Hz.

When the FR service is provided by the inverter interfaced RES, frequency dynamics of the system can be notably improved. All the three FR strategies can effectively raise the frequency nadir of the system; among them, the PD control has the best performance, and increases the frequency nadir to 49.72 Hz during the transient. At the same time, these FR schemes also suppress the maximum level of the RoCoF. When the PD control and the inertia control are used, the maximum RoCoF levels of the system are substantially suppressed to 0.17 and 0.23 Hz/s, respectively, indicating a much slower rate of system frequency drop. RoCoF suppression under the droop control is less obvious.

Besides, when the droop control or the PD control is adopted, the steady-state frequency is increased. Conversely, the inertia control fails to improve the steady-state frequency, which maintains 49.79 Hz as in the natural response case.

VI. Conclusion

As the penetration level of RES increases, the equivalent inertia and damping of power system decrease drastically. This causes negative impact on grid FR characteristics, and makes it necessary for the inverters to provide the FR service in order to ensure the safety and stability of the grid frequency.

In this manuscript, under the consistent constraint of the inverter available FR capacity, the effects of different FR strategies on the suppression of $\Delta\omega$ and RoCoF are discussed. Specifically, it is proven that the droop and the PD controls can effectively reduce the maximum $\Delta\omega$ to the same level if their optimal conditions are satisfied, whereas the inertia control is incapable of controlling the maximum $\Delta\omega$. The inertia control and the PD control effectively reduce the maximum RoCoF to the same level if both operated optimally, yet the droop control lacks such an ability.

Besides, the practical implementations of controllers vary for strategies. For the droop and inertia controls, it is virtually impossible to design for optimal FR performances due to difficulty in obtaining pertinent parameters, yet the optimal PD control can be constantly realized by exploiting the full idle capacity of the inverter regardless of the unknown parameters.

References

[1] L. Xiong, X. Liu, Y. Liu, and F. Zhuo, "Modeling and stability issues of voltage-source converter dominated power systems: A review," *CSEE J. Power Energy Syst.*, to be published, doi: 10.17775/CSEE-JPES.2020.03590.

[2] X. Zeng, T. Liu, S. Wang *et al.*, "Comprehensive coordinated control strategy of pmsg-based wind turbine for providing frequency regulation services," *IEEE Access*, vol. 7, pp. 63 944–63 953, Sep. 2019.

[3] L. Xiong, L. Liu, X. Liu, and Y. Liu, "Frequency trajectory planning based strategy for improving frequency stability of droop-controlled inverter based standalone power systems," *IEEE J. Emerg. Sel. Top. Circuits Syst.*, vol. 11, no. 1, pp. 176–187, 2021.

[4] K. S. Ratnam, K. Palanisamy, and G. Yang, "Future low-inertia power systems: Requirements, issues, and solutions-A review," *Renew. Sust. Energ. Rev.*, vol. 124, p. 109773, 2020.

[5] X. Zeng, T. Liu, S. Wang *et al.*, "Coordinated control of mmc-hvdc system with offshore wind farm for providing emulated inertia support," *IET Renew. Power Gener.*, vol. 14, pp. 673–683, May. 2020.

[6] W. Wu, Y. Chen, A. Luo *et al.*, "A virtual inertia control strategy for DC microgrids analogized with virtual synchronous machines," *IEEE Trans. Ind. Electron.*, vol. 64, no. 7, pp. 6005–6016, 2016.

[7] H. Nguyen, G. Yang, A. Nielsen, and P. Jensen, "Combination of synchronous condenser and synthetic inertia for frequency stability enhancement in low-inertia systems," *IEEE Trans. Sustain. Energy*, vol. 10, no. 3, pp. 997–1005, 2019.

[8] H.-P. Beck and R. Hesse, "Virtual synchronous machine," in *Proc. 9th Int. Conf. Elect. Power Qual. Utilisation*, pp. 1–6, 2007.

[9] Q.-C. Zhong and G. Weiss, "Synchronverters: Inverters that mimic synchronous generators," *IEEE Trans. Ind. Electron.*, vol. 58, no. 4, pp. 1259–1267, 2010.

[10] W. Zhang, D. Remon, and P. Rodriguez, "Frequency support characteristics of grid-interactive power converters based on the synchronous power controller," *IET Renew. Power Gener.*, vol. 11, no. 4, pp. 470–479, 2016.

[11] X. Meng, J. Liu, and Z. Liu, "A generalized droop control for grid-supporting inverter based on comparison between traditional droop control and virtual synchronous generator control," *IEEE Trans. Power Electron.*, vol. 34, no. 6, pp. 5416–5438, 2018.

[12] M. A. Torres L., L. A. C. Lopes, L. A. Morán T., and J. R. Espinoza C., "Self-tuning virtual synchronous machine: A control strategy for energy storage systems to support dynamic frequency control," *IEEE Trans. Energy Convers.*, vol. 29, no. 4, pp. 833–840, 2014.

[13] D. Terazono, J. Liu, Y. Miura *et al.*, "Grid frequency regulation support from back-to-back motor drive system with virtual-synchronous-generator-based coordinated control," *IEEE Trans. Power Electron.*, vol. 36, no. 3, pp. 2901–2913, 2021.

[14] S. D'Arco and J. A. Suul, "Equivalence of virtual synchronous machines and frequency-droops for converter-based microgrids," *IEEE Trans. Smart Grid*, vol. 5, no. 1, pp. 394–395, 2013.
[15] A. Attya, J. L. Dominguez-Garcia, and O. Anaya-Lara, "A review on frequency support provision by wind power plants: Current and future challenges," *Renew. Sustain. Energy Rev.*, vol. 81, pp. 2071–2087, 2018.
[16] Y. Ye, Y. Qiao, and Z. Lu, "Revolution of frequency regulation in the converter-dominated power system," *Renew. Sustain. Energy Rev.*, vol. 111, pp. 145–156, 2019.
[17] C. Phurailatpam, Z. H. Rather, B. Bahrani, and S. Doolla, "Measurement-based estimation of inertia in AC microgrids," *IEEE Trans. Sustain. Energy*, vol. 11, no. 3, pp. 1975–1984, 2020.
[18] L. Xiong, F. Zhuo, F. Wang *et al.*, "Static synchronous generator model: a new perspective to investigate dynamic characteristics and stability issues of grid-tied PWM inverter," *IEEE Trans. Power Electron.*, vol. 31, no. 9, pp. 6264–6280, Sep. 2016.
[19] E. Spahic, D. Varma, G. Beck *et al.*, "Impact of reduced system inertia on stable power system operation and an overview of possible solutions," in *Proc. 2016 IEEE Power Energy Soc. Gen. Meeting*, pp. 1–5, 2016.
[20] J. Fang, H. Li, Y. Tang, and F. Blaabjerg, "Distributed power system virtual inertia implemented by grid-connected power converters," *IEEE Trans. Power Electron.*, vol. 33, no. 10, pp. 8488–8499, 2018.
[21] Y. Li, Z. Xu, and K. P. Wong, "Advanced control strategies of pmsgbased wind turbines for system inertia support," *IEEE Trans. Power Electron.*, vol. 32, no. 4, pp. 3027–3037, 2017.
[22] B. Kroposki, B. Johnson, Y. Zhang *et al.*, "Achieving a 100% renewable grid: Operating electric power systems with extremely high levels of variable renewable energy," *IEEE Power Energy Mag.*, vol. 15, no. 2, pp. 61–73, 2017.
[23] J. Fang, Y. Tang, H. Li, and X. Li, "A battery/ultracapacitor hybrid energy storage system for implementing the power management of virtual synchronous generators," *IEEE Trans. Power Electron.*, vol. 33, no. 4, pp. 2820–2824, 2018.
[24] E. Hammad, A. M. Khalil, A. Farraj *et al.*, "A class of switching exploits based on inter-area oscillations," *IEEE Trans. Smart Grid*, vol. 9, no. 5, pp. 4659–4668, 2018.